J Fluoresc (2009) 19:997–1008
DOI 10.1007/s10895-009-0499-2

ORIGINAL PAPER

Effect of Pendant Group Length Upon Metal Ion Complexation in Acetonitrile by Di-Ionized Calix[4] Arenes Bearing Two Dansyl Fluorophores

Ümmühan Ocak · Miraç Ocak · Xin Shen · Kazimierz Surowiec · Richard A. Bartsch

Received: 14 February 2009 / Accepted: 5 June 2009 / Published online: 25 June 2009

Abstract A series of three di-ionizable calix[4]arenes with two pendant dansyl (1-dimethylaminonaphthalene-5-sulfonyl) groups linked to the lower rims was synthesized. Structures of the three ligands were identical except for the length of the spacers which connected the two dansyl groups to the calix[4]arene scaffold. Following conversion of the ligands into their di-ionized di(tetramethylammonium) salts, absorption and emission spectrophotometry were utilized to probe the influence of metal cation (Li^+, Na^+, K^+, Rb^+, Cs^+, Mg^{2+}, Ca^{2+}, Sr^{2+}, Ba^{2+}, Ag^+, Cd^{2+}, Co^{2+}, Fe^{2+}, Hg^{2+}, Mn^{2+}, Pb^{2+}, Zn^{2+} and Fe^{3+}) complexation in acetonitrile. Upon complexation with these metal cations, emission spectra underwent marked red shifts and quenching of the dansyl group fluorescence for the di-ionized ligand with the shortest spacer. A similar effect was noted for the di-ionized ligand with an intermediate spacer for all of the metal ions, except Ba^{2+}. For the di-ionized ligand with the longest spacer, the metal cations showed different effects on the emission spectrum. Li^+, Mg^{2+}, Ca^{2+} and Ba^{2+} caused enhancement of emission intensity with a red shift. Other metal cations produce quenching with red shifts in the emission spectra. Transition metal cations interacted strongly with all three di-ionized ligands. In particular, Fe^{3+} and Hg^{2+} caused greater than 99% quenching of the dansyl fluorescence in the di-ionized ligands.

Ü. Ocak · M. Ocak · X. Shen · K. Surowiec · R. A. Bartsch
Department of Chemistry and Biochemistry,
Texas Tech University,
Lubbock, TX 79409, USA

Ü. Ocak (✉) · M. Ocak
Department of Chemistry, Faculty of Arts and Sciences,
Karadeniz Technical University,
61080 Trabzon, Turkey
e-mail: uocak@ktu.edu.tr

Keywords Calixarene ligand · Fluorescence spectroscopy · Stability constant · Metal ion complexation

Introduction

Due to their toxicity, the detection of heavy metal ions with fluorescent chemosensors has attracted considerable interest [1–5]. These compounds have been prepared by attachment of fluorophore moieties to the frameworks of macrocyclic or chelating ligands. One sensing mechanism is macrocyclic complexation with a metal cation [6, 7]. Complexation may produce a change in the response of the fluorescent group with either an increase or decrease in intensity. Also, a shift in the fluorescence spectrum of the chemosensor may be observed upon interaction of the macrocyclic moiety with the cation.

Calixarenes are a class of macrocyclic compounds formed by phenol-formaldehyde condensation with well-defined upper and lower rims and a central annulus. The calixarenes are able to act as host molecules due to their bucket-shaped cavities. Substituted calix[4]arenes are capable of binding various cations on the lower rim or on the upper rim [8–12]. Because of these properties calix[4]arenes have considerable potential as a basic platform for the design of fluorescent chemosensors. Recently, various chemosensors based on calix[4]arenes bearing fluorescent groups have been synthesized for investigation of their fluorescent responses upon complexation with various metal cations [13–15].

The dansyl group and its derivatives are frequently employed as fluorescent groups in chemosensors for metal cation detection and determination [16–18]. Dansyl-modified calix[4]arenes exhibit variation of fluorescence intensity upon addition of a metal cation in solution [19,

20]. Valeur and coworkers reported a highly sensitive and selective fluorescent molecular sensor for Pb^{2+} based on a calix[4]arene with four dansyl groups on the lower rim [17]. A calix[4]arene-based fluorescent chemosensor bearing four dansyl amides on the upper rim was reported by Huang and coworkers to show high sensitivity and selectivity toward Hg^{2+} [21]. The conformation of the calixarene scaffold is frequently important for effective complexation [22, 23]. Kumar reported a dansyl group-containing, fluorescent chemosensor based on a calix[4] arene in the partial cone conformation for recognition of Hg^{2+} and Cu^{2+} [24]. Cation-arene interaction may also be important for complexation [25].

In an earlier study, we reported the interaction of di-ionized ligand **L1** (Scheme 1) with metal cations using spectrophotometric and spectrofluorimetric methods [26]. In this paper, we report the synthesis of new calix[4]arene ligands **2** and **3** (Scheme 1). The structures of ligands **1–3** differ in having one, three and four methylene groups in the spacers by which the dansyl amide moieties are attached to the lower rim of the calix[4]arene scaffold. The influence of such systematic structural variation can provide insight into how the ligands interact with metal ions. Responses of di(tetramethylammonium) salts of the di-ionizable ligands **1–3** to a variety of metal cations are assessed by spectrofluorometric titrations in acetonitrile. The complex stability constants and complex compositions of Hg^{2+}, Pb^{2+} and Fe^{3+} with the three ionized ligands are determined. In this study, we compare the results of interaction of di-ionized ligand **L1** with Li^+, Na^+, K^+, Rb^+, Cs^+, Mg^{2+}, Ca^{2+}, Sr^{2+}, Ba^{2+}, Ag^+, Cd^{2+}, Co^{2+}, Fe^{2+}, Hg^{2+}, Mn^{2+}, Pb^{2+}, Zn^{2+} and Fe^{3+} with those of the new di-ionized ligands **L2** and **L3** in which spacer length is increased.

Experimental

Chemicals

Acetonitrile from EM (spectrometric grade) was the solvent for absorption and fluorescence measurements. All metal perchlorates purchased from Acros were of the highest quality available and vacuum dried over blue silica gel before use.

Apparatus

^{1}H NMR spectra were measured in $CDCl_3$ at 500 MHz with a Varian Unity INOVA spectrometer. IR spectra were recorded with a Perkin-Elmer model 1600 FT-IR spectrophotometer. Absorption spectra were recorded on a Shimadzu model 2401PC UV-visible spectrophotometer. Fluorescence spectra were obtained on a SLM Aminco 8000C photon counting spectrofluorometer equipped with a 450-W ozone-free xenon lamp as the light source. Combustion analysis was performed by Desert Analytics Laboratory of Tucson, Arizona.

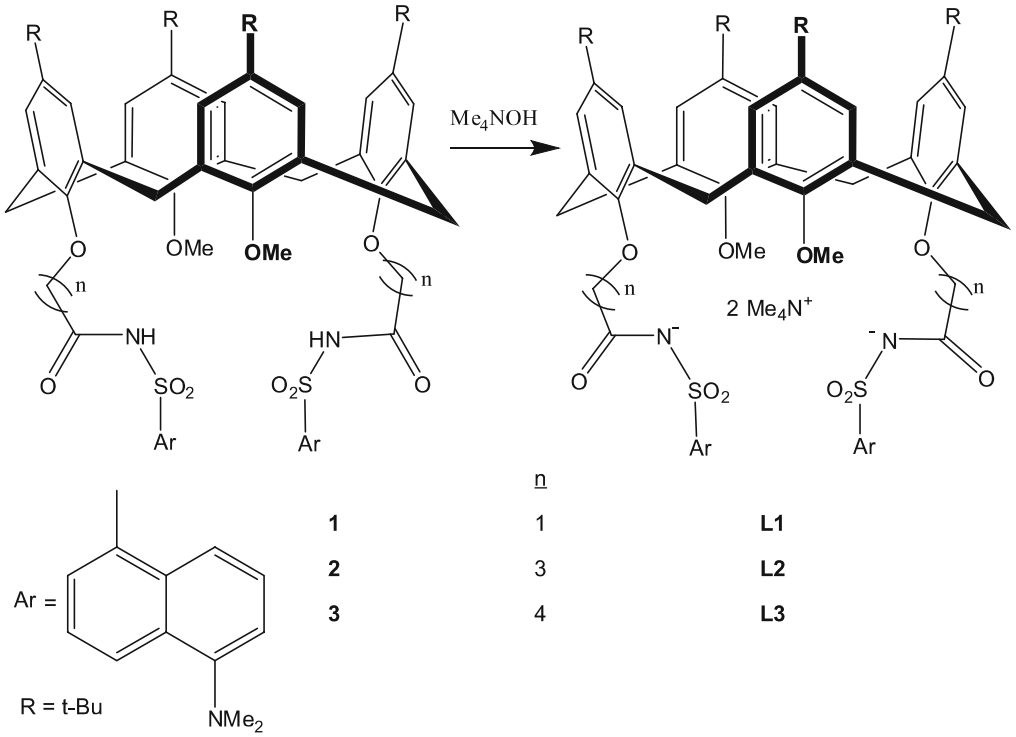

Scheme 1 Structures of ionophores **1–3** and their di-ionized tetramethylammonium salts **L1–L3**, respectively

Absorption and fluorescence measurements

Absorption spectra of the di-ionized ligands (2.58×10^{-5} M) in acetonitrile solutions containing 50 molar equivalents of the appropriate metal perchlorate salt were measured using a 1-cm absorption cell. Fluorescence spectra of the same solutions were measured with a 1-cm quartz cell. The excitation wavelength was 328 nm for all the ionized ligands. Fluorescence emission spectra were recorded in the range 400–750 nm with a slit width of 1.0 nm.

The stoichiometries of the complexes and their stability constants were determined according to a literature procedure [27].

Ligand synthesis

The 25,27-dimethoxycalix[4]arene (**4**) [28] and 5,11,17,23-tetrakis(1,1-dimethylethyl)-25,27-bis[N-(5′-dimethylaminonaphthalene-1′-sulfonyl]carbamoylmethoxy)-26,28-dimethoxycalix-[4]arene (**1**) [29] were prepared according to reported procedures.

General procedure for preparation of 5,11,17,23-tetrakis (1,1-dimethylethyl)-25,27-bis[3-(ethoxycarbonyl)propoxy]-26,28-dimethoxycalix[4]arene (**5**) and 5,11,17,23-tetra-kis (1,1-dimethylethyl)-25,27-bis[4-(ethoxycarbonyl)butoxy]-26,28-dimethoxycalix[4]-arene (**6**). To a suspension of NaH (0.96 g, 50 mmol) in DMF (100 ml), **4** (4.52 g, 10 mmol) was added and the mixture was stirred at room temperature. When the evolution of hydrogen ceased, a solution of ethyl 3-bromobutanoate (for **5**) or ethyl 5-bromopentanoate (for **6**) (22 mmol) in DMF (5 ml) was added over a period of 0.5 h. The mixture was stirred for an additional 2 h and then the excess of NaH was decomposed by dropwise addition of water. The mixture was diluted with 1 N HCl (200 ml) and extracted with CH_2Cl_2 (2×200 ml). The combined organic layers were washed with water, dried with $MgSO_4$,

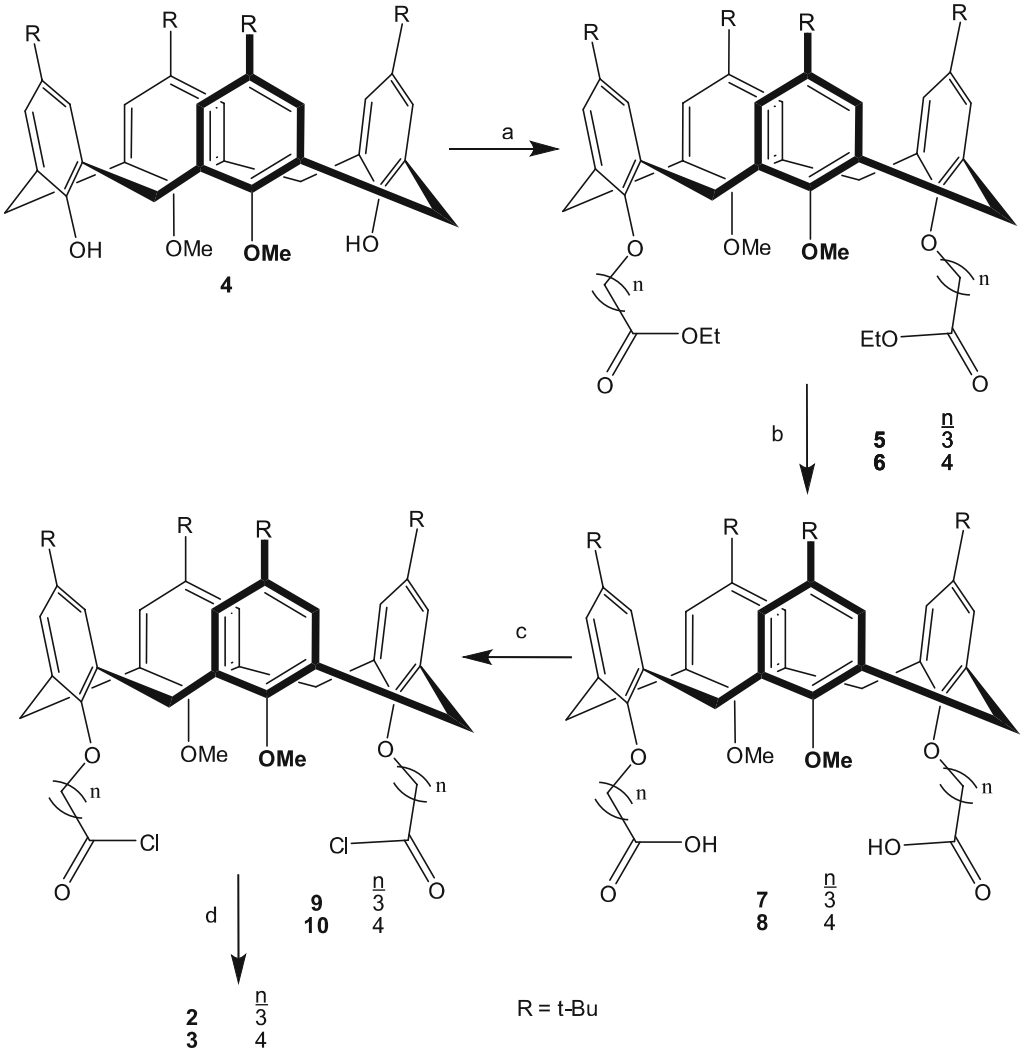

Scheme 2 Synthetic route to di-ionizable calix[4]arenes **2** and **3**: **a** NaH and $Br(CH_2)_nCO_2C_2H_5$, DMF, room temperature; **b** 10% aqueous Me_4NOH, THF, reflux; **c** $(COCl)_2$, benzene, reflux; **d** NaH, dansyl amide, THF, room temperature

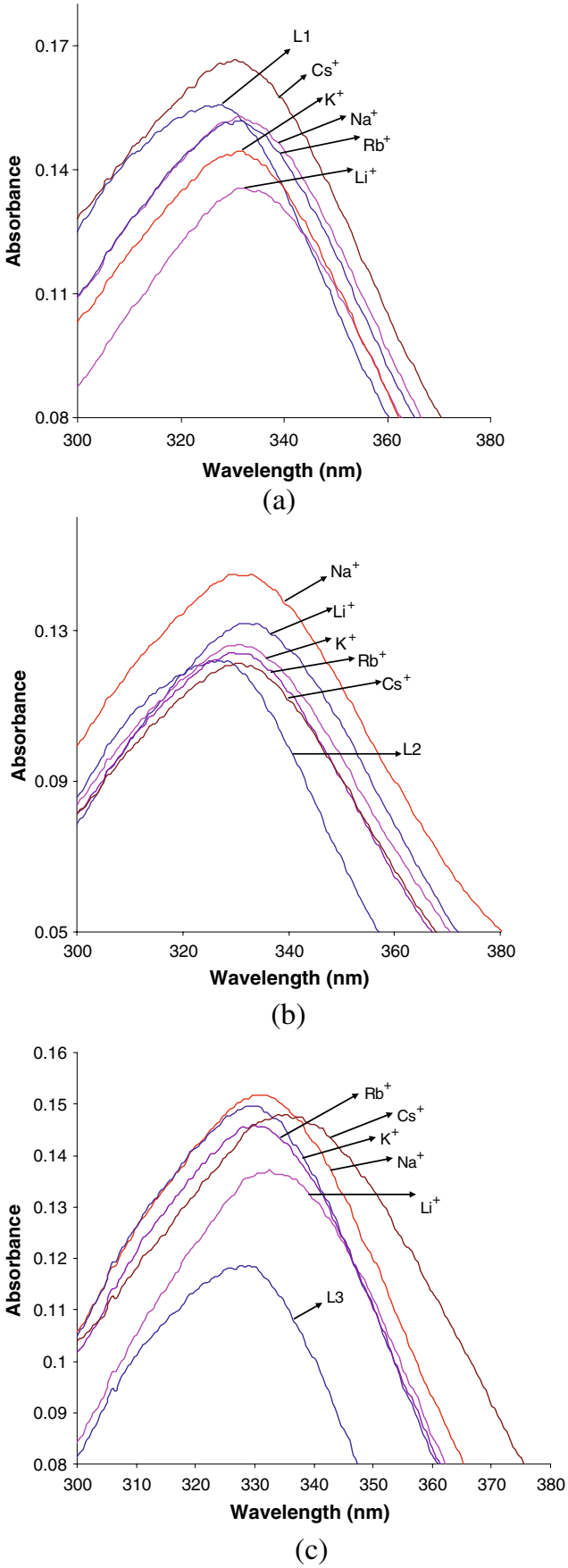

and evaporated *in vacuo*. The DMF and most of the excess alkylating agent were removed by distillation under vacuum (60 °C, 1 Torr). The residual pale yellow oil was purified by column chromatography on silica gel with hexanes-EtOAc (40:1) as eluent to give the final product.

For **5**, 86% yield of white solid with mp 109–111 °C. IR (deposit from CH_2Cl_2 solution on a NaCl plate): 1736 (C=O) cm^{-1}. ^1H NMR (500 MHz, $CDCl_3$): δ 0.80 (br s, 9H), 1.04 (br s, 9H), 1.26 (t, J=7.2 Hz, 6H), 1.34 (br d, J= 24.8, 18H), 2.16–4.31 (m, 30H), 6.30–7.24 (m, 8H). Anal. Calcd. for $C_{58}H_{80}O_8$: C, 76.95; H, 8.91. Found: C, 77.08; H, 8.79.

For **6**, 76% yield of colorless oil. IR (film): 1737 (C=O) cm^{-1}. ^1H NMR (500 MHz, $CDCl_3$): δ 0.80 (br s, 9H), 1.04 (br s, 9H), 1.25 (t, J=7.1 Hz, 6H), 1.29–1.41 (m, 18H), 1.71–4.20 (m, 34 H), 6.20–7.25 (m, 8H). Anal. Calcd. for $C_{60}H_{84}O_8$: C, 77.21; H, 9.07. Found: C, 77.41; H. 8.93

General procedure for preparation of 5,11,17,23-tetrakis (1,1-dimethylethyl)-25,27-bis(3-carboxypropoxy)-26,28-dimethoxycalix[4]arene (**7**) and 5,11,17,23-tetrakis(1,1-dimethylethyl)-25,27-bis(4-carboxybutoxy)-26,28-dimethoxycalix [4]arene (**8**). A solution of diester **7** or **8** (5.0 mmol), THF (150 ml), and 10% aqueous Me_4NOH (150 ml) was refluxed overnight. The mixture was acidified with 2 N HCl (100 ml) and extracted with CH_2Cl_2 (2×200 ml). The combined organic extracts were washed with water, dried over $MgSO_4$, and evaporated *in vacuo* to give the product.

For **7**, 97% yield of white solid with mp 254–256 °C. IR (deposit from CH_2Cl_2 solution on a NaCl plate): 3300–2420 (CO_2H), 1711 (C=O) cm^{-1}. ^1H NMR (500 MHz, $CDCl_3$): δ 0.60–1.60 (m, 36H), 2.10–4.16 (m, 26H), 6.35–7.60 (m, 8H). Anal. Calcd. for $C_{54}H_{72}O_8$•$0.6CH_2Cl_2$: C, 72.88; H, 8.20. Found: C, 72.74; H, 7.95.

For **8**, 97% yield of white solid with mp 233–235 °C. IR (deposit from CH_2Cl_2 solution on a NaCl plate): 3620–2420 (CO_2H), 1711 (C=O) cm^{-1}. ^1H NMR (500 MHz, $CDCl_3$): δ 0.70–1.19 (m, 18H), 1.36 (br s, 18H), 1.72–2.54 (m, 12H), 2.93–3.37 (m, 6H), 3.42–4.43 (m, 12H), 6.35–6.66 (m, 4H), 6.82–7.27 (m, 4H). Anal. Calcd. for $C_{56}H_{76}O_8$, C, 76.68; H, 8.73. Found: C, 76.83; H, 9.00.

General procedure for preparation of 5,11,17,23-tetrakis (1,1-dimethylethyl)-25,27-bis[3-(N-(5′-dimethylaminonaphthalene-1′-sulfonyl)carbamoypropoxy]-26,28-dimethoxy-calix [4]arene (**2**) and 5,11,17,23-tetrakis(1,1-dimethylethyl)-25,27-bis[4-(N-(5′-dimethyl-aminonaphthalene-1′-sulfonyl)carbamoylbutoxy]-26,28-dimethoxycalix[4]arene (**3**). The diacid **7** (1.50 g, 1.77 mmol) or **8** (1.50 g, 1.71 mmol) was dried by azeotropic distillation of a benzene solution using a Dean-Stark trap. To the dried solution, oxalyl chloride (10 molar

◀ **Fig. 1** Effect of alkali metal cations on the absorption spectra of **L1**–**L3** in acetonitrile: **a** for **L1**; **b** for **L2**; and **c** for **L3**

equivalents) was added and the solution was refluxed for 5 h under nitrogen. The benzene and excess oxalyl chloride were evaporated *in vacuo* to produce the crude di(acid chloride), which was used directly in the next step without purification. Under nitrogen, dansyl amide (7.08 mmol) was added to a mixture of NaH (0.42 g, 17.7 mmol) and THF (100 ml) and the mixture was stirred at room temperature for 3 h, followed by the dropwise addition of a solution of the di(acid chloride) in THF (10 ml). The mixture was stirred at room temperature for an additional 24 h, then water was carefully added to destroy the excess of NaH. The THF was evaporated *in vacuo* and the aqueous residue was acidified with 1 N HCl. The mixture was extracted with CH_2Cl_2 (2×100 ml). The combined extracts were washed with water, dried over $MgSO_4$ and evaporated *in vacuo*. The residue was purified by column chromatography on silica gel with CH_2Cl_2-MeOH (80:1) as eluent.

For **2**, 81% yield of a light green solid with mp 160–175 °C. IR (deposit from CH_2Cl_2 solution on a NaCl plate): 3250 (NH), 1727 (C=O), 1359 and 1171 (SO_2) cm^{-1}. ^1H NMR (500 MHz, $CDCl_3$): δ 0.85–1.40 (m, 36H), 2.00 (br s, 4H), 2.40–4.22 (m, 42H), 6.75 (br s, 4H), 7.03 (s, 4H), 7.10 (d, J=7.5 Hz, 2H), 7.48 (t, J=7.5 Hz, 2H), 7.58 (t, J=7.5 Hz, 2H), 8.23 (d, J= 10.0 Hz, 2H), 8.52 (d, J=7.0 Hz, 2H), 8.58 (d, 10.0 Hz, 2H), 9.66 (br s, 2H). Anal. Calcd. for $C_{78}H_{96}N_4O_{10}S_2$: C, 71.31; H, 7.37; N, 4.26. Found: C, 71.67; H, 7.09; N, 4.49.

For **3**, 81% yield of a light green solid with mp 174–191 °C. IR (deposit from CH_2Cl_2 solution on a NaCl plate: 3236 (NH), 1718 (C=O), 1360 and 1170 (SO_2) cm^{-1}. ^1H NMR (500 MHz, $CDCl_3$): δ 0.60–1.42 (m, 36H), 1.55–4.40 (m, 42H), 6.25–7.68 (m, 14H), 8.03–8.78 (m, 6H), 9.75 (br s, 2H). Anal. Calcd. for $C_{80}H_{100}N_4O_{10}S_2$•0.2$CDCl_3$: C, 70.52; H, 7.41; N, 4.10. Found: C, 70.75; H, 7.36; N, 4.00.

Preparation of the di(tetramethylammonium) salts of the di-ionized ligands

The di(tetramethylammonium) salts of ligands **1**–**3** were prepared by adaptation of a published procedure [26].

Results and discussion

Ligand synthesis

New di-ionizable calix[4]arene ligands **2** and **3** were prepared as shown in Scheme 2. Distally dimethylated *tert*-butylcalix[4]arene **4** was reacted with sodium hydride and then with ethyl 4-bromobutanoate or ethyl 5-bromopentanoate to produce diesters **5** and **6**, respectively. Basic hydrolysis of **5** and **6** gave di(carboxylic acids) **7** and **8**, respectively. Reactions of **7** and **8** with oxalyl chloride produced the corresponding di(acid chlorides) **9** and **10** which were reacted with the sodium salt of dansyl amide to give ligands **2** and **3**, respectively. Structures of new calix [4]arene compounds **2**, **3**, and **5**–**8** were verified by ^1H NMR spectroscopy, IR spectrophotometry, and combustion analysis.

Ligands **1**–**3** were transformed into their di-ionized tetramethylammonium salts **L1**–**L3** by reaction with aqueous tetramethylammonium hydroxide in benzene (Scheme 1).

For ligands **1**–**3** and their di-ionized tetramethylammonium salts **L1**–**L3**, the number of methylene groups in the spacer which joins the dansyl amide groups to the calix[4] arene framework is systematically varied from one to three to four. Due to the propensity for a reverse Michael reaction, an analogue with two methylene groups in the spacer is not synthetically feasible.

Absorption spectra

In acetonitrile, **L1**–**L3** exhibit an absorption band with a maximum at 328 nm. Molar absorption coefficients were 6.0×10^3, 4.7×10^3 and 4.6×10^3 cm^{-1} M^{-1} for di-ionized ligands **L1**–**L3**, respectively, at this wavelength maximum.

The presence of 50 equivalents of alkali metal cations produced pronounced decreases with red shifts in the absorption of **L1** at 328 nm, except for Cs^+. As the largest alkali metal cation examined, Cs^+ caused an enhancement in absorption with a red shift. The data in Fig. 1a show the largest absorption decrease for Li^+ among the alkali metal cations. It is interesting that the effect of alkali metal cations on the absorption spectra of **L2** (Fig. 2b) are reversed from those observed for **L1**. Namely, alkali metal cations produced pronounced enhancements with red shifts in the absorption of **L2** at 328 nm, except for Cs^+. Cs^+ caused a modest absorption decrease with a red shift at this wavelength. For **L2**, the greatest enhancement was observed with Na^+ among the alkali metal cations. The effects of alkali metal cations on the absorption spectra of **L3**, which has the longest spacer between the dansyl amide group and the calix[4]arene framework, are different than those for **L1** and **L2**. For **L3**, all of the alkali metal cations produced pronounced enhancements in the intensity of the 328 nm absorption band (Fig. 1c). Like **L2**, the greatest enhancement was observed with Na^+. There were red shifts of 2–7 nm for all of the alkali metal cations. The largest red shift of 7 nm was noted for Cs^+. These results show that the length of the pendant groups on the lower rim influences how the ligands interact with alkali metal cations.

Figure 2 shows the effect of alkaline earth metal cations on the absorption spectra of **L1**, **L2**, and **L3** in acetonitrile. A red shift of the 328 nm absorption of **L1** was observed for all of the alkaline earth metal cations (Fig. 2a). For **L1**–**L3**, the largest red shifts of 7–11 nm were found for Mg^{2+}. Larger red shifts for alkaline earth metal cations compared

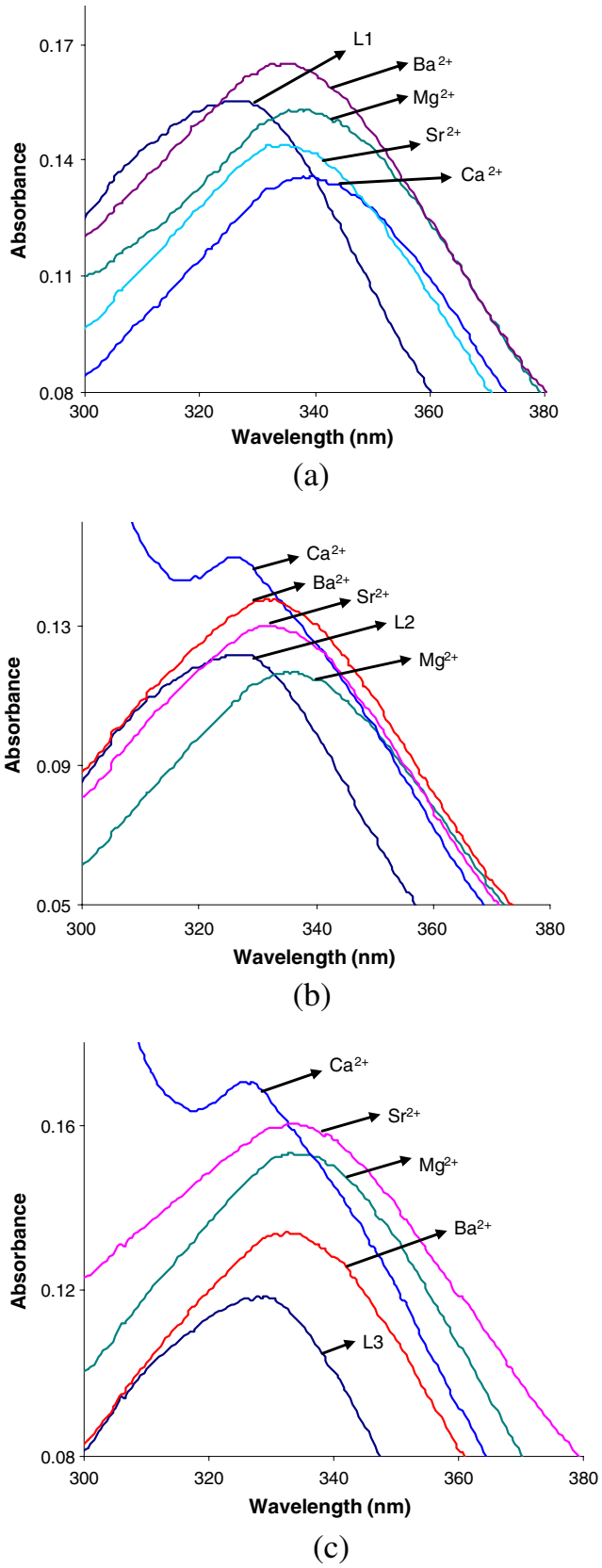

Fig. 2 Effect of alkaline earth metal cations on the absorption spectra of **L1**–**L3** in acetonitrile: **a** for **L1**; **b** for **L2**; and **c** for **L3**

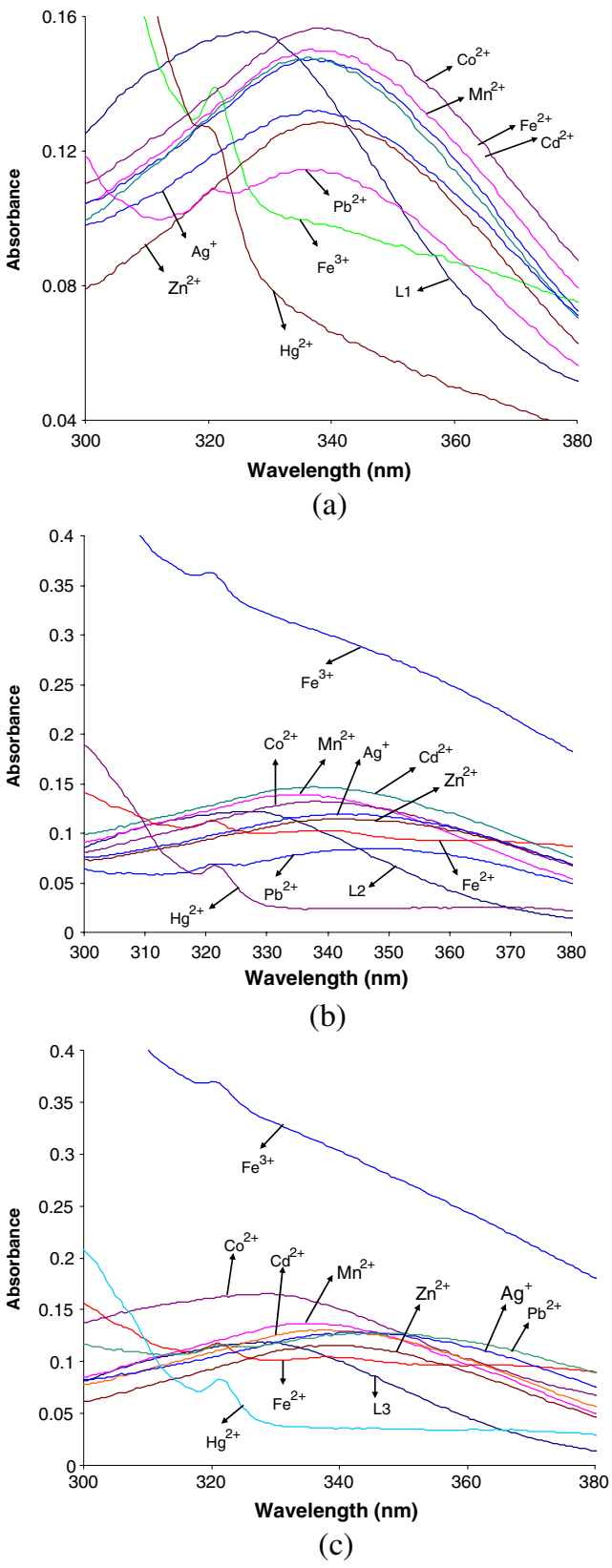

Fig. 3 Effect of transition metal cations and Pb^{2+}on the absorption spectra of **L1**–**L3** in acetonitrile: **a** for **L1**; **b** for **L2**; and **c** for **L3**

with alkali metal cations result from their higher charge density. This result is the same as that reported previously for a structurally related series of calix[4]arene ligands [26]. Mg^{2+}, Ca^{2+}, and Sr^{2+} produced decreases in the absorption of **L1**, whereas Ba^{2+} caused enhancement. As noted above for alkali metal cations, only the largest of the alkaline earth metal cations gave absorption enhancement for **L1**. For **L2**, there were red shifts and absorption enhancements with all of the alkaline earth metal cations, except Mg^{2+} for which there was a decrease in absorption with a red shift (Fig. 2b). For **L3**, all of the alkaline earth metal cations produced pronounced absorptions enhancements with red shifts for Mg^{2+}, Sr^{2+}, and Ba^{2+} (Fig. 2c). Ca^{2+} produced a small blue shift and exhibited the largest absorption enhancement. As can be seen from the data in Fig. 2, the spacer lengths for the pendant groups on the lower rim differentiate the effect of alkaline earth metal cations on the absorption spectra. In particular, the spectral shape is different for Ca^{2+} in the case of **L2** and **L3** compared with **L1**. A new absorption band was observed at about 324 nm for the di-ionized ligands **L2** and **L3**. Absorption enhancement below 320 nm for both ligands in the case of Ca^{2+} is also evident. These results suggest that the interaction mechanism of Ca^{2+} with **L2** and **L3** is similar, but differ from that of **L1**.

Figure 3 shows the effect of transition metal cations and Pb^{2+} on the absorption spectra of **L1**–**L3** in acetonitrile. Red shifts were observed for Ag^{+}, Cd^{2+}, Co^{2+}, Fe^{2+}, Mn^{2+}, $Pb^{2+}$and Zn^{2+} on the absorption spectrum of **L1** (Fig. 3a). Effects of Hg^{2+} and Fe^{3+} on the absorption spectra of **L1** were found to be different from those for other transition metal cations. Hg^{2+} and Fe^{3+} produced new absorption maxima at about 323 nm, which are similar in shape to those for Ca^{2+} with **L2** and **L3**. For Pb^{2+} and **L1**, there was only a small change in absorption intensity. Except for Co^{2+}, the absorption spectra of **L2** and **L3** in the presence of 50 equivalents of transition metal cations and Pb^{2+} are very similar (compare Fig. 3b and c). There is an absorption enhancement in the spectrum of **L3** with Co^{2+}, which is not evident for **L2**. The effect of Fe^{3+} on the absorption spectra of **L1** differs markedly from those for **L2** and **L3**. Fe^{3+} caused an absorption decrease for **L1** (Fig. 3a), whereas it gave strong enhancements in the absorption spectra of **L2** and **L3** (Fig. 3b and c, respectively). These results reveal that the interaction mechanism of Fe^{3+} with **L2** and **L3** is similar, but differs from that for **L1**.

The observed red shifts can be explained as resulting from photoinduced charge transfer. Cation binding results in enhancement of photoinduced charge transfer from the dimethyamine group on the dansyl fluorophore to the

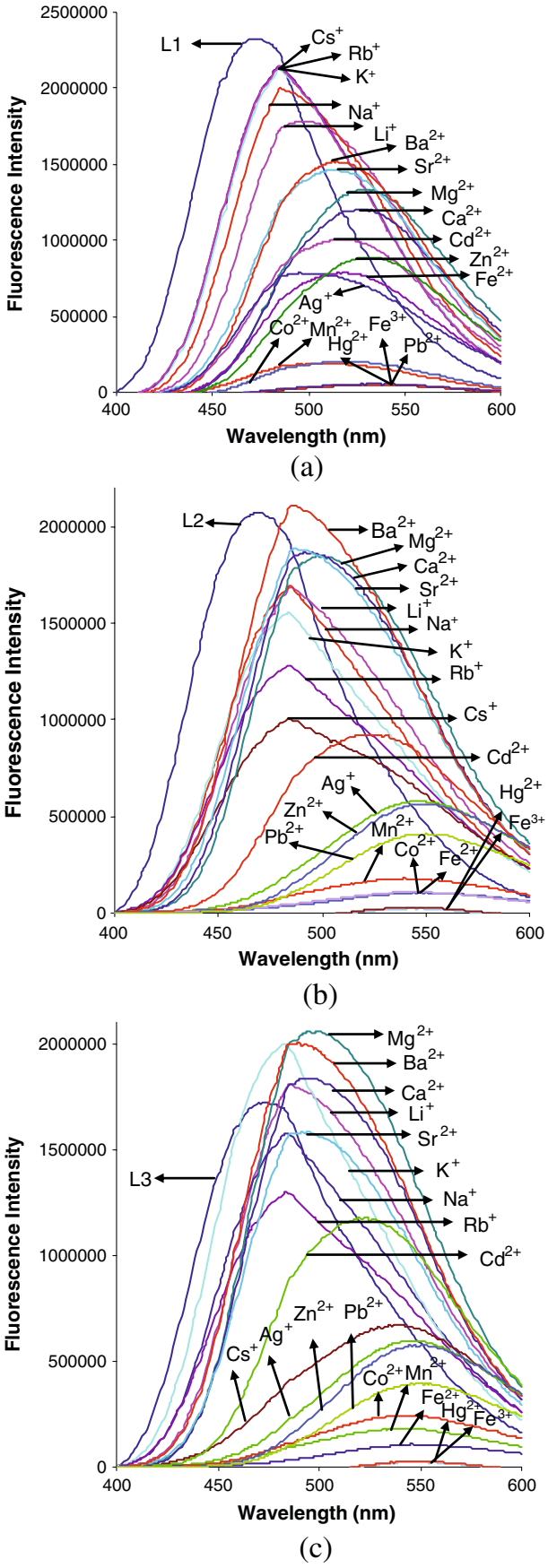

Fig. 4 Effect of metal cations on the emission spectra of **L1**–**L3** in acetonitrile: **a** for **L1**; **b** for **L2**; and **c** for **L3**

carbonyl group. Consequently, a red shift is observed in the absorption spectra.

Fluorescence spectra

When excited at 328 nm, **L1**, **L2**, and **L3** gave emission bands with maxima at 473, 470 and 472 nm, respectively. Figure 4 shows the effects of metal cations on the fluorescence spectra of **L1**–**L3**. The emission band intensities for **L1** were reduced somewhat by the presence of alkali metal cations and diminished substantially for interactions with alkaline earth metal cations (Fig. 4a). Also, dramatic red shifts of the emission band were observed in the presence of Li^+, Na^+, K^+, Rb^+, Cs^+, Mg^{2+}, Ca^{2+}, Sr^{2+} and Ba^{2+}. Strong quenching of the fluorescence emission was observed with the transition metal cations of Ag^+, Cd^{2+}, Co^{2+}, Fe^{2+}, Mn^{2+} and Zn^{2+}. Even stronger quenching was noted with Pb^{2+}, Hg^{2+}, and Fe^{3+}. The observed quenching for heavy metal cations, such as Hg^{2+} , Cd^{2+}, and Pb^{2+}, probably results from the "heavy atom effect" [30].

Figure 4b shows the effects of metal cations on the fluorescence spectra of the di-ionized calix[4]arene **L2**. As can be seen, adding two more methylene groups to the spacer that links the pendent dansyl groups with the lower rim of **L1** alters the effect of metal cations on the fluorescence spectra. For **L2**, the influence of Mg^{2+}, Ca^{2+}, and Sr^{2+} was nearly the same with red shifts and moderate quenching. On the other hand, Ba^{2+} produced a red shift but essentially no quenching for the emission spectrum of **L2**. On the other hand, Cs^+ gave the largest quenching for the series of alkali metal cations. This result shows that Cs^+ interacts with the di-ionized ligand **L2** more strongly when compared to the other alkali metal cations. Transition metal cations cause pronounced quenching of the emission spectrum of **L2**. However the quenching produced by Pb^{2+} in the fluorescence spectra of **L2** is less than that for **L1**. Hg^{2+} and Fe^{3+} caused greater than 99% quenching of the dansyl fluorescence in the di-ionized ligand **L2**.

Figure 4c shows the effects of metal cations on the fluorescence spectra of the di-ionized ligand **L3**. From comparison of Fig. 4b and c, it can be seen that the presence Sr^{2+} produced similar levels of emission quenching for **L2** and **L3**. However, the other alkaline earth metal cations caused enhanced fluorescence emission when the ligand was changed from **L2** to **L3**. This result reveals that the interaction mechanism for Mg^{2+}, Ca^{2+}, and Ba^{2+} with the two ligands is different that for Sr^{2+}. The effects of transition metal cations and Pb^{2+} on the fluorescence spectra of di-ionized ligand **L3** are quite similar to those for **L2.**

The relationship between the magnitude of the red shifts for the fluorescence emission and the metal ion diameters for **L1**–**L3** is presented in Fig. 5. There is a good correlation between the magnitude of the red shifts and

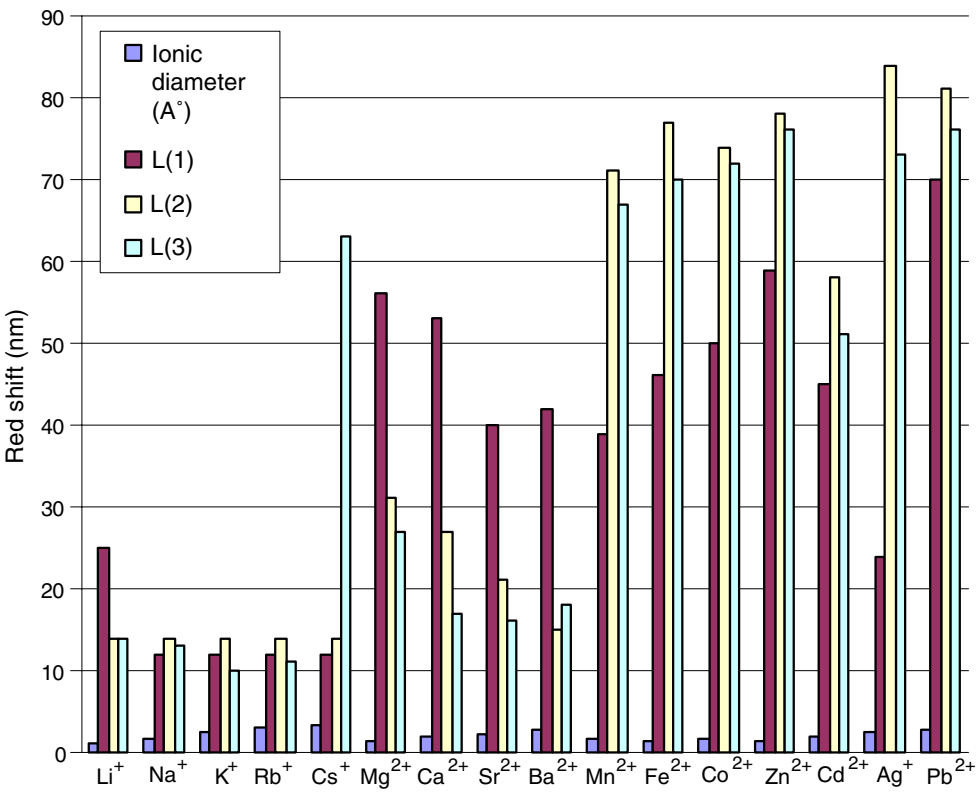

Fig. 5 Bar chart of the red shift of the fluorescence emission observed as a function of the metal ion diameter at 473, 470, and 472 nm for **L1**, **L2**, and **L3**, respectively

the alkaline earth metal cation diameters for **L2**. Thus decreasing the ionic diameter causes a larger red shift. The other ligands show similar relationships, except for Ba^{2+}. Among the alkaline earth metal cations, the largest red shifts were found for Mg^{2+} for all three ligands. Among the alkali metal cations, Cs^{+} showed the largest red shift of 63 nm for **L3**. It is interesting to note that there are regular increases in the red shift for **L1** and **L3** with the first row transition metal cations of Mn^{2+}, Co^{2+}, Fe^{2+}, and Zn^{2+}, respectively, The magnitudes of the red shifts increased in the order **L1** < **L3** < **L2** for the heavy metal cations of Ag^{+}, Cd^{2+}, and Pb^{2+}. The largest red shift of 84 nm was observed for Ag^{+} and **L2**.

The number of methylene groups in the space which joins the dansyl amide groups to the calixarene framework does not significantly affect the values of red shifts produced by Na^{+}, K^{+}, and Rb^{+}. However, the red shift for Cs^{+} was strongly influenced by the number of methylene groups in the spacer. Di-ionized ligand **L3** with the longest spacer showed about six times the red shift compared with those for **L2** and **L1**. Similarly, increasing the number of methylene groups in the spacer from one to three or four enhanced the red shift produced with Ag^{+} by nearly four times.

Figure 6 presents the relative changes of fluorescence efficiency at the wavelength of maximum emission for the three di-ionized ligands. Quenching was observed for all metal cations in the case of **L1**. Similarly, there was quenching for all metal cations, except for Ba^{2+}, in the case of **L2**. Transition metal cations and Pb^{2+} produced stronger fluorescence quenching for all three of the di-ionized ligands. It is interesting to note that the orders of quenching efficiency were $Li^{+}>Na^{+}>K^{+}>Rb^{+}\approx Cs^{+}$ and $Li^{+}\approx Na^{+}<K^{+}<Rb^{+}<Cs^{+}$ for **L1** and **L2**, respectively. Thus, there is an exactly reversed relationship between quenching efficiency and cationic diameter when the ligand was changed from **L1** to **L2**. On the other hand, **L3** showed increases in the fluorescence intensity for Li^{+}, K^{+}, Mg^{2+}, Ca^{2+}, and Ba^{2+}. The other metal cations produced quenching of the fluorescence intensity for **L3**. As shown in Fig. 6, Fe^{3+} and Hg^{2+} caused greater than 99% quenching of the dansyl fluorescence for the di-ionized ligands **L1**–**L3**. In the presence of Pb^{2+}, the quenching efficiency of **L1** was about 98%.

Determination of stability constants

Stability constants and stoichiometries for complexation of Hg^{2+}, Pb^{2+}, and Fe^{3+} by **L1**–**L3** was determined by fluorimetric titration. The titration experiments were performed by adding solutions with various concentrations of the metal perchlorate in acetonitrile to solutions of the di-ionized ligand in the same solvent. The ligand concentration was held constant at 2.58×10^{-5} M. The stoichiometries of the complexes and their stability constants were determined from changes in the fluorescence intensity as a function of the metal ion concentration. Successive decreases of emission with increases of the metal ion concentration were observed in all of the fluorimetric titrations.

Figure 7 shows the fluorescence spectra of **L2** in acetonitrile with increasing concentrations of Pb^{2+}. The inserts are plots of the change of fluorescence intensity *vs.*

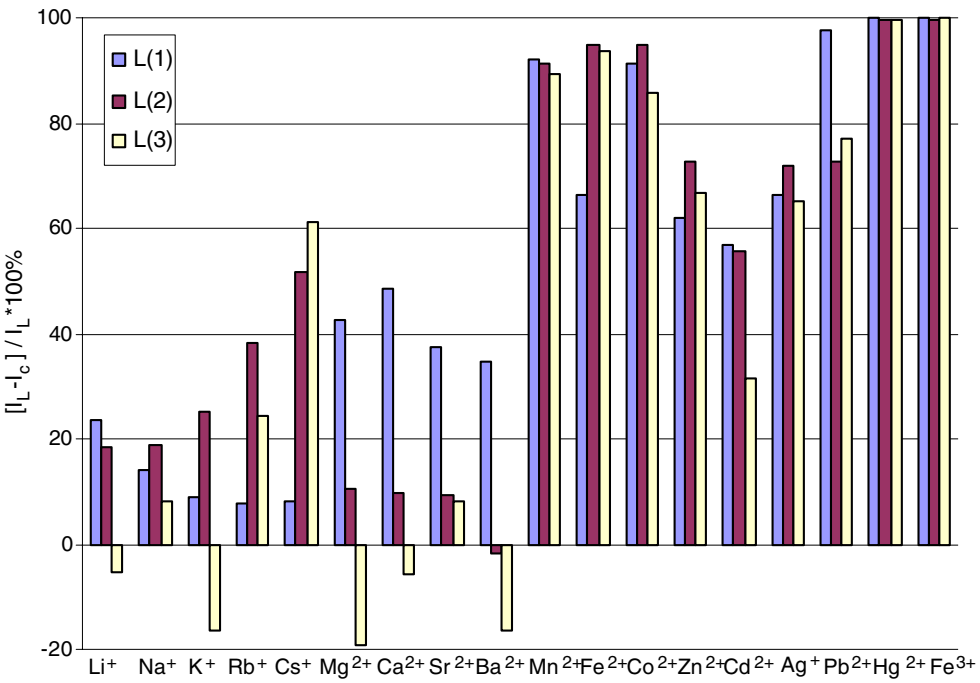

Fig. 6 Bar chart of quenching efficiency for different metal ions observed at the wavelength of maximum emission for the di-ionized ligands **L1**, **L2**, and **L3**

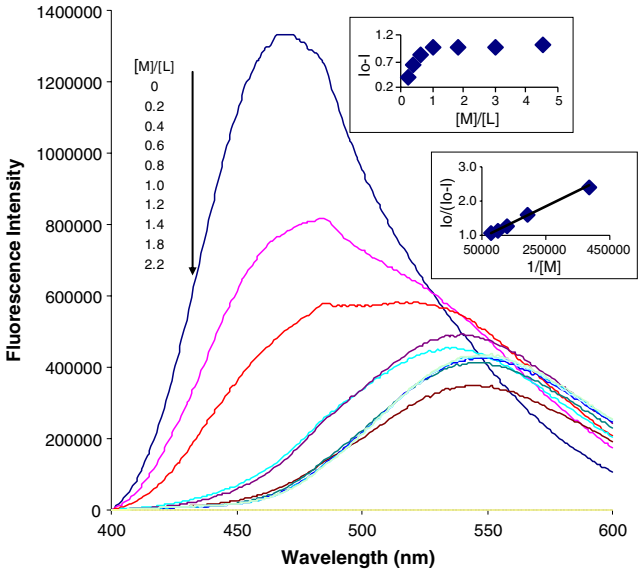

Fig. 7 Fluorescence spectra (λ_{exc}:328 nm, λ_{em}:470 nm) of **L2** in acetonitrile with increasing amounts of Pb^{2+} and [**L2**]=2.58×10^{-5} M. See text for description of insets

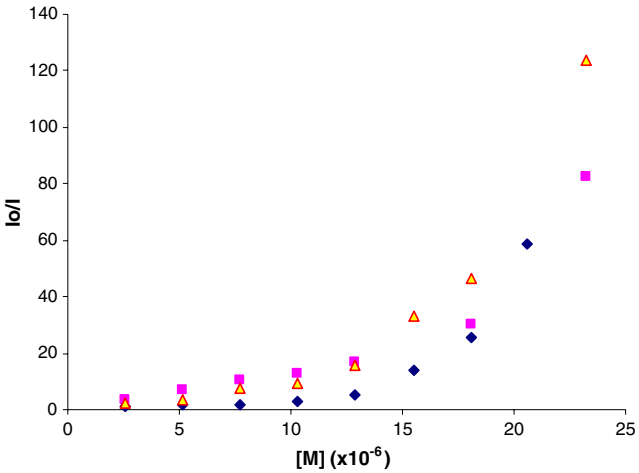

Fig. 8 Stern-Volmer plots for quenching of the di-ionized ligands (2.58×10^{-5} M) in acetonitrile by Hg^{2+}: diamonds = **L1**; squares = **L2**; and triangles = **L3**

the ratio of [metal ion]/[ligand] and a plot of the quantity $I_0/(I_0\text{-}I)$ versus [metal ion]$^{-1}$. The break in the first curve at [metal ion]/[ligand] = 1.0 provides strong evidence for formation of a 1:1 complex. Similar plots were found for **L3** with Hg^{2+}, Pb^{2+}, and Fe^{3+}. In an earlier study, 1:1 complexation of these three metal ions with **L1** was established [26]. In the current study, we found a 1:1 complex of Pb^{2+} with **L2**. However, Hg^{2+} and Fe^{3+} gave 1:2 (M:L) complexes with the same ligand. Thus **L2** shows a different conformational arrangement during the complexation with Hg^{2+} and Fe^{3+} cations. Stability constants of the complexes were determined from plots of the quantity $I_0/(I_0\text{-}I)$ versus [metal ion]$^{-1}$. The ratio of intercept/slope gave the stability constants [27].

Table 1 presents the calculated stability constants and the complex stochiometries of **L1**, **L2**, and **L3** with Fe^{3+}, Hg^{2+}, and Pb^{2+}. The log β values of 3.84–5.99 demonstrate strong interactions of these metal ions with the di-ionized ligands in acetonitrile. Among the three ligands, **L3** gave the most stable complex with a log β value of 5.67 for Pb^{2+}. As can be seen from the data in Table 1, increasing the number of methylene groups in the spacers produced enhancement of the log β value for complexation of Pb^{2+}. However, **L2** had the largest stability constant for Fe^{3+} and Hg^{2+}. Most stable is the Hg^{2+} complex of **L2** which had a log β value of 5.99. On the other hand, **L1** was the weakest ligand for these three metal ions.

Stern-Volmer analysis

Stern-Volmer analysis was utilized to probe the nature of the quenching process in the complexation of Fe^{3+}, Hg^{2+}, and Pb^{2+} by **L1**–**L3**. Stern-Volmer plots are a useful method of presenting data on emission quenching [31, 32]. From the data, dynamic or static quenching processes can be determined. Plotting relative emission intensities (I_o/I) against quencher concentration [Q] for a static process should yield a linear Stern-Volmer plot. Expressed as Eq. 1, the slope of the plotted line yields Ksv, the static quenching constant.

$$I_o/I = 1 + Ksv[Q] \quad (1)$$

Figure 8 shows the steady-state emission Stern-Volmer analysis for Hg^{2+} and ligands **L1**–**L3**. In all cases,

Table 1 Stability constants and complex stochiometries for complexes of di-ionized calixarenes **L1**, **L2**, and **L3** with Hg^{2+}, Pb^{2+} and Fe^{3+} in acetonitrile

	Stability constant (Log β)			Complex stochiometry (M:L)		
	Cation			Cation		
Di-ionized ligand	Fe^{3+}	Hg^{2+}	Pb^{2+}	Fe^{3+}	Hg^{2+}	Pb^{2+}
L1	4.06±0.02[a]	3.84±0.01[a]	4.43±0.03[a]	1:1[a]	1:1[a]	1:1[a]
L2	5.96±0.03	5.99±0.04	5.24±0.02	1:2	1:2	1:1
L3	5.40±0.05	5.64±0.03	5.67±0.01	1:1	1:1	1:1

[a] From reference [26]

nonlinear behavior with positive deviations from the typically linear Stern-Volmer analysis was observed. Similar results were obtained for Fe^{3+} and Pb^{2+}. These results indicate that both static and dynamic quenching are taking place.

Acknowledgments This work was supported by The Scientific and Technological Research Council of Turkey (TUBITAK). We also thank the Division of Chemical Sciences, Geosciences and Biosciences of the Office of Basic Energy Sciences of the U.S. Department of Energy (Grant DE-FG02-90ER14416) for support of this research.

References

1. Valeur B, Leray I (2000) Design principles of fluorescent molecular sensors for cation recognition. Coord Chem Rev 205:3–40. doi:10.1016/S0010-8545(00)00246-0
2. Valeur B, Leray I (2007) Ion-responsive supramolecular fluorescent systems based on multichromophoric calixarenes: a review. Inorg Chim Acta 360:765–774. doi:10.1016/j.ica.2006.07.027
3. Zhou Y, Xiao Y, Qian X (2008) A highly selective Cd^{2+} sensor of naphthyridine: fluorescent enhancement and red-shift by the synergistic action of forming binuclear complex. Tetrahedron Lett 49:3380–3384. doi:10.1016/j.tetlet.2008.03.128
4. He G, Zhao Y, He C, Liu Y, Duan C (2008) "Turn-on" fluorescent sensor for Hg^{2+} via displacement approach. Inorg Chem 47:5169–5176. doi:10.1021/ic702494s
5. Lv J, Ouyang C, Yin X, Zheng H, Zuo Z, Xu J, Liu H, Li Y (2008) Reversible and highly selective fluorescent sensor for mercury(II) based on a water-soluble poly(para-phenylene)s containing thymine and sulfonate moieties. Macromol Rapid Commun 29:1588–1592. doi:10.1002/marc.200800256
6. Álvaro M, García H, Palomares E, Achour R, Moussaif A, Zniber R (2001) A bis-benzimidazole-derived N,S macrocycle as sensor for transition metal ions in aqueous solution. Chem Phys Lett 350:240–246. doi:10.1016/S0009-2614(01)01302-1
7. Ng PL, Lee CS, Kwong HL, Chan ASC (2005) Zinc complex of bipyridine crown macrocycle: luminescence sensing of anions in aqueous media via the cooperative action of metal-ligand and hydrophobic interactions. Inorg Chem Commun 8:769–772. doi:10.1016/j.inoche.2005.05.014
8. Israeli Y, Detellier C (1997) Complexation of the sodium cation by a calix[4]arene tetraester in solution. Formation of a 2:1 calixarene:sodium complex. J Phys Chem B 101:1897–1901. doi:10.1021/jp962538q
9. Danylyuk O, Lazar AN, Coleman AW, Suwinska K (2008) A novel structural motif for calix[4]arene dihydrophosphonic acid in its complex with dimethylammonium and tetramethylammonium cations. J Mol Struct 891:404–407. doi:10.1016/j.molstruc.2008.04.022
10. Liu JM, Zheng QY, Yang JL, Chen CF, Huang ZT (2002) A new fluorescent chemosensor for Fe^{3+} and Cu^{2+} based on calix[4]arene. Tetrahedron Lett 43:9209–9212. doi:10.1016/S0040-4039(02)02265-7
11. Ludwig R, Dzung NTK (2002) Calixarene-based molecules for cation recognition. Sensors 2:397–416. doi:10.3390/s21000397
12. Petrella AJ, Raston CL (2004) Calixarenes as platforms for the construction of multimetallic complexes. J Organomet Chem 689:4125–4136. doi:10.1016/j.jorganchem.2004.07.065
13. Penf Q, Tang XH (2009) Synthesis of a novel calix[4]arene-based fluorescent ionophore and its metal ions recognition properties. Chin Chem Lett 20:13–16. doi:10.1016/j.cclet.2008.09.062
14. Kim SK, Kim SH, Kim HJ, Lee SH, Lee SW, Ko J, Bartsch RA, Kim JS (2005) Indium(III)-Induced fluorescent excimer formation and extinction in calix[4]arene-fluoroionophores. Inorg Chem 44:7866–7875. doi:10.1021/ic050702v
15. Prodi L, Pivari S, Bolletta F, Hissler M, Ziessel R (1998) Synthesis of functionalized calix[4]arene ligands incorporating bipyridine N,N'-dioxide chromophores and luminescence of their lanthanide complexes. Eur J Inorg Chem, 1959–1965. doi:10.1002/(SICI)1099-0682(199812)1998:12<1959::AID-EJIC1959>3.0.CO;2-0
16. Chen QY, Chen CF (2005) A new Hg^{2+}-selective fluorescent sensor based on a dansyl amide-armed calix[4]-aza-crown. Tetrahedron Lett 46:165–168. doi:10.1016/j.tetlet.2004.10.169
17. Metivier R, Leray I, Valeur B (2003) A highly sensitive and selective fluorescent molecular sensor for Pb(II) based on a calix[4]arene bearing four dansyl groups. Chem Commun (Camb), 996–997. doi:10.1039/b301323e
18. Pandey S, Azam A, Pandey S, Chawla HM (2009) Novel dansyl-appended calix[4]arene frameworks: fluorescence properties and mercury sensing. Org Biomol Chem 7:269–279. doi:10.1039/b815379e
19. Narita M, Higuchi Y, Hamada F, Kumagai H (1998) Metal sensor of water soluble dansyl-modified thiacalix[4]arenes. Tetrahedron Lett 39:8687–8690. doi:10.1016/S0040-4039(98)01899-1
20. Talanova GG, Roper ED, Buie NM, Gorbunova MG, Bartsch RA, Talanov VS (2005) Novel fluorogenic calix[4]arene-bis(crown-6-ether) for selective recognition of thallium(I). Chem Commun (Camb) 45:5673–5675. doi:10.1039/b510348g
21. Li GK, Liu M, Yang GQ, Chen CF, Huang ZT (2008) An effective Hg^{2+}-selective fluorescent chemosensor based on a calix[4]arene bearing four dansyl amides. Chin J Chem 26:1440–1446. doi:10.1002/cjoc.200890262
22. Gutsche CD (1989) Calixarenes. Royal Society of Chemistry, Cambridge, England
23. Jose P, Menon S (2007) Lower rim substituted calixarenes and their applications. J Bioinorg Chem Appl, 7/1–7/16
24. Dhir A, Bhalla V, Kumar M (2008) Ratiometric sensing of Hg^{2+} based on the calix[4]arene of *partial cone* conformation possessing a dansyl moiety. Org Lett 10:4891–4894. doi:10.1021/ol801984y
25. Gerosa AZ, Solari E, Giannini L, Floriani C, Villab AC, Rizzoli C (1997) Shaping the cavity of calix[4]arene using transition metals and binding alkali-metal cations inside the cavity: the relevance of the alkali-metal cation–arene interaction. Chem Commun (Camb), 183–184. doi:10.1039/a606826j
26. Ocak Ü, Ocak M, Surowiec K, Bartsch RA, Gorbunova MG, Tu C, Surowiec MA (2009) Metal ion complexation in acetonitrile by di-ionized calix[4]arenes bearing two dansyl fluorophores. J Incl Phenom Macrocycl Chem 63:131–139. doi:10.1007/s10847-008-9497-2
27. Bourson J, Valeur B (1989) Ion-responsive fluorescent compounds. Cation-steered intramolecular charge transfer in a crowned merocyanine. J Phys Chem 93:3871–3876. doi:10.1021/j100346a099
28. Van Loon J-D, Arduini A, Coppi L, Verboom W, Pochini A, Ungaro R, Harkema S, Reinhoudt DN (1990) Selective functionalization of calix[4]arenes at the upper rim. J Org Chem 55:5639–5646. doi:10.1021/jo00308a024
29. Talanova GG, Elkarim NSA, Talanov VS, Bartsch RA (1999) A calixarene-based fluorogenic reagent for selective mercury(II) recognition. Anal Chem 71:3106–3109. doi:10.1021/ac990205u
30. Aragoni MC, Arca N, Bencini A, Blake AJ, Caltagirone C, Danesi A, Devillanova FA, Garau A, Gelbrich T, Isaia F, Lippolis V, Hursthouse MB, Valtancoli B, Wilson C (2007) New fluorescent

chemosensors for heavy metal ions based on functionalized pendant arm derivatives of 7-anthracenylmethyl-1, 4, 10-trioxa-7, 13-diazacyclopentadecane. Inorg Chem 46:8088–8097. doi:10.1021/ic700657j

31. Murphy CB, Zhang Y, Troxler T, Ferry V, Martin JJ, Jones WE (2004) Probing Förster and Dexter energy-transfer mechanisms in fluorescent conjugated polymer chemosensors. J Phys Chem B 108:1537–1543. doi:10.1021/jp0301406
32. Larsen RW, Helms MK, Everett WR, Jameson DM (1999) Ground- and excited-state characterization of an electrostatic complex between tetrakis(4-sulfanato-phenyl)porphyrin and 16-pyrimidinium crown-4. Photochem Photobiol 69:429–434